Mechanics of Advanced Composite Structures

Journal homepage: https://macs.semnan.ac.ir/

Semnan University

ISSN: 2423-7043

Research Article

Asymmetric and Oblique Impact on Perforated Plates and Ceramic–Composite Armor Systems: A Numerical Study

Hamd Rajab, Tayebeh Akbari *, Ali Davar, Jafar Eskandari Jam

Faculty of Materials & Manufacturing Technologies, Malek Ashtar University of Technology, Tehran, Iran

ARTICLE INFO

Article history:

Received: 2023-10-19
Revised: 2024-03-22
Accepted: 2024-05-12

Keywords:

Zigzagged Silicon Carbide;
Perforated plate;
Asymmetric impact.

ABSTRACT

This study focuses on the design and development of an advanced armor system that combines perforated steel plates and ceramic with a zigzag geometry to enhance ballistic protection. The objective is to provide effective defense against high-velocity armor-piercing threats while maintaining lightweight characteristics. The armor system consists of a perforated steel plate integrated with a base made of zigzagged silicon carbide (SiC), aluminum, and Kevlar. The novel aspect of this design lies in the modification of the ceramic surface, where a contoured geometry is implemented to increase energy absorption and projectile deflection upon impact. Additionally, conical perforations are introduced in the steel plate to enhance asymmetric impact behavior, contributing to the armor's ability to deflect or fragment incoming projectiles. Finite Element Analysis (FEA) using LS-DYNA simulations and design of experiment software were employed to determine the optimal geometric configuration of the perforations and ceramic surface. This analysis focused on parameters such as the angle of the conical hole, the arrangement and thickness ratio of the aluminum and Kevlar layers, and the air gap between the perforated plate and the base armor. The results indicate that the combination of the perforated steel plate and the modified ceramic surface significantly improves ballistic performance by enhancing the armor's capacity to dissipate impact energy and prevent penetration. The developed system demonstrates its effectiveness in protecting against armor-piercing threats while offering a lightweight solution for military and civilian defense applications.

1. Introduction

In recent years, the increasing prevalence of armor-piercing projectiles has posed a significant threat to both military personnel and civilian populations. Traditional armor systems, while effective, often compromise between weight and protection, making them less viable for modern applications where mobility and comfort are essential. Consequently, there is an urgent need for innovative armor solutions that can effectively counter high-velocity threats while minimizing weight [1].

Oblique impact plays a critical role in ballistic impact research, as projectiles typically impact targets at varying angles of obliquity. The oblique impact plays a crucial role in determining the target's ballistic resistance. Numerous studies in the literature address the normal and oblique impacts of armor systems [2] and metal [3] structures, highlighting the influence of impact angles on their protective performance. These studies collectively demonstrate that oblique impacts significantly alter failure mechanisms, emphasizing the necessity of considering non-normal impact conditions in armor design.

For example, research from Biswas et al. [2] provides insights into how residual velocities and ballistic limits alter under varied oblique impact conditions, revealing critical thresholds at which impact resistance either shifts to embedding the projectile or prompts a ricochet effect. This work underscores the sensitivity of

* **Corresponding author.**
E-mail address: t.akbari.k@gmail.com

Cite this article as:
Mohammadi, A. and Mahdi-Nia, M., 2025. Title of article. *Mechanics of Advanced Composite Structures*, 12(1), pp. xx-xx
https://doi.org/10.22075/MACS.2024.39315.2050

ballistic response to the impact angle, validating the importance of studying asymmetric conditions.

Recent research has increasingly focused on the use of sandwich and hybrid composite structures to enhance impact resistance and energy absorption—key characteristics also desired in advanced armor systems. Taghipoor et al. [4] investigated the behavior of glass fiber/polyester layered composites under low-velocity impact, highlighting the crucial role of material layering and matrix–fiber interaction in enhancing energy absorption and structural integrity. In a related study, Taghipoor et al. [5] conducted an experimental investigation on corrugated-core sandwich panels under impact loading, demonstrating that panel thickness and multi-core configurations play a vital role in improving crashworthiness and specific energy absorption (SEA). In a related study, Taghipoor et al. [6] explored the performance of polyurethane foam-core sandwich panels reinforced with Kevlar/epoxy facesheets, emphasizing that the arrangement and number of composite layers have a significant influence on total absorbed energy and damage mechanisms. Furthermore, Taghipoor et al. [7] examined the low-velocity impact response of Kevlar/epoxy-polyurethane sandwich structures and found that fiber orientation and impactor geometry greatly affect maximum energy absorption and deformation behavior. Collectively, these recent studies highlight the growing potential of hybrid composite and sandwich configurations in dissipating impact energy—supporting the current study's approach to developing lightweight, multi-layered armor systems with enhanced ballistic resistance.

Shokrieh et al. [8] conducted a numerical investigation to evaluate the impact behavior of a boron carbide–Kevlar 49/epoxy protection system under a 30° oblique impact. The results revealed that bullet corrosion was more significant in inclined impact conditions compared to normal impact. Additionally, the study demonstrated that the ballistic limit velocity at a 30° inclined angle was higher than that observed under normal impact conditions. This suggests that angled impacts may increase the effective ballistic limit of composite systems due to extended projectile path lengths.

Jiang et al. [9] analyzed the penetration resistance of a specially engineered ceramic/metal composite armor, which was fabricated using a semi-cylindrical ceramic-metal backplate. Its effectiveness against a 12.7 mm armor-piercing incendiary projectile was evaluated through both experimental and numerical methods. The findings indicate that significant positional deviation during projectile penetration leads to distinct penetration behavior compared to conventional symmetric composite armor. Stanisławek et al. [10] conducted a numerical investigation on the impact behavior of a multilayer composite panel subjected to an AP (Armor Piercing) 14.5 × 114 mm B32 projectile. The composite panel was composed of alternating layers of ceramic pyramids and a ductile aluminum alloy. The performance of these models was compared to a reference structure, a conventional double-layer panel. The study utilized modeling and simulation techniques, including the finite element method implemented in LS-DYNA software. A key finding of this research was the significant deviation in projectile trajectory, which was highly dependent on the impact location. This demonstrates how geometric asymmetry in armor design can alter projectile trajectory and energy dissipation.

One promising approach in composite armor design is the integration of perforated steel plates, which induce projectile deflection and fragmentation, thereby reducing their penetration ability. Studies have shown that perforated plates are particularly effective in dissipating the energy of small-caliber projectiles and can enhance multi-hit resistance [11]. Mubashar et al. [12] examined the ballistic performance of a specially designed perforated armor plate against a 12.7 mm armor-piercing tracer projectile. The findings indicated that perforations with a 9 mm diameter generated adequate bending stresses to fracture the projectile's core, which is the primary mechanism for preventing penetration. Conversely, perforation diameters that were either smaller or larger failed to induce core fracture, reducing the armor's effectiveness against AP projectiles. Hao et al. [13] investigated the hole arrangement and shape on the ballistic behavior and failure mode of a perforated structure. Different impact speeds involving three domains of the velocity value, two types of hole arrangements, and three hole geometries (i.e., square, triangle, and circle). Analysis of both numerical and experimental results consistently highlighted asymmetric ballistic effects, primarily attributed to impacts occurring near the hole edges. Anshun et al. [14] conducted ballistic tests to evaluate the protective performance of various perforated steel plates against a 12.7 mm armor-piercing shell. The study analyzed key factors, including the residual penetration depth of different base armors, the damaged area of the perforated plates, and the frequency of core fractures. The results revealed a linear relationship between projectile deflection angle and the material properties of perforated steel plates. Specifically, harder perforated plates with circular holes

exhibited greater core deflection. Additionally, plates with hexagonal perforations induced even higher core deflection compared to those with circular holes, highlighting the influence of hole geometry on projectile deviation. Their study supports the role of hole geometry and distribution in controlling asymmetric impact behavior.

The study aimed to assess the software's capability in replicating ballistic impact effects and evaluating steel plate armor performance. The numerical analysis confirmed that various constitutive models effectively captured the qualitative behavior of the physical mechanisms involved in perforation. For practical applications, selecting an appropriate constitutive model and fracture criterion within the finite element method (FEM) demonstrated strong agreement with experimental results, reinforcing the accuracy of LS-DYNA in simulating projectile impacts on steel targets. Given the advances in hybrid armor technologies, this study focuses on the design and numerical simulation of an armor system consisting of perforated steel plates (additional armor) and zigzagged SiC ceramics, aluminum, and Kevlar (base armor). The goal is to optimize the system's performance against 12.7 mm AP tracer rounds, with particular attention paid to the geometry of the perforated plates, material arrangement, and aluminum-to-Kevlar thickness ratio within the armor structure. By leveraging recent advances in both materials science and numerical modeling, the integration of simulation models such as FEM and RSM in recent studies enables the precise design and optimization of these armor systems, ensuring their adaptability to a variety of combat scenarios. Finally, this research aims to provide a comprehensive solution for modern ballistic protection.

2. Research Materials and Methods

This work uses numerical simulation to design and develop an armor protection system consisting of a lightweight composite armor (Zigzag aluminum / Zigzag SiC Ceramic/ Aluminum / Kevlar) and a perforated armor plate made of Armox 500T for 12.7 mm threats. The geometrical configuration of the ceramic, Kevlar, and perforated plate will be determined based on the numerical study (LS-DYNA). The proposed hole pattern of the perforated plate is conical, and its arrangement type is dislocation. The proposed ceramic configuration is a zigzag surface. The response surface methodology (RSM) determines the geometrical parameters, such as the thickness of the aluminum and Kevlar layers.

2.1. Numerical Simulations

The numerical analysis of the ballistic response of the protection system is conducted using LS-DYNA software. The computational model must accurately capture the rapid variations in total internal energy, pressure, density, and temperature that occur ahead of the impact wave [15]. A crucial aspect of this modeling is the equation of state (EOS), which defines the thermodynamic relationship between pressure, temperature, and density for the materials under investigation. In this study, the Mie-Grüneisen EOS framework is employed to simulate the behavior of the perforated plate, aluminum plate, and projectile, ensuring a precise representation of pressure distribution and shock wave propagation within the numerical simulations. The pressure response in the Mie-Grüneisen EOS model [16] under pressure is given by:

$$P = \begin{cases} \dfrac{\rho_0 C_0^2 \mu \left[1 + \left(1 - \frac{\gamma_0}{2}\right)u - \frac{a}{2}\mu^2\right]}{\left[1 - (S_1 - 1)\mu - S_2 \frac{\mu^2}{\mu+1} - S_3 \frac{\mu^3}{(\mu+1)^2}\right]^2} \\ \quad +(\gamma_0 + a\mu)E \qquad (\mu \geq 0) \\ \rho_0 C_0^2 \mu + (\gamma_0 + a\mu)E \qquad (\mu < 0) \end{cases} \tag{1}$$

where P represents the pressure, S_1, S_2, and S_3 denote the slant coefficients of the particle velocity - shock velocity relationship. The parameter γ_0 corresponds to the Grüneisen coefficient, and (a) is the first-order volume correction factor associated with γ_0, and ρ_0 denotes the initial density of the material. Additionally, C represents the Hugoniot intercept of the particle velocity - shock velocity curve, while E denotes the absolute internal energy. The parameter μ is the specific volume, defined as $\mu = \rho/\rho_0 - 1$, and ρ is the immediate density of the material under hydrostatic compression. The Mie-Grüneisen EOS model parameters for a perforated plate, Al 5083-H116, and the projectile are provided in **Error! Reference source not found.**. The Johnson-Cook strain-rate sensitive model is utilized to characterize the compressive strength of materials subjected to high-strain rates and large deformations. This constitutive model effectively captures the strain hardening, strain-rate dependency, and thermal softening effects, making it particularly suitable for ballistic impact and high-speed deformation simulations [15].

Table 1. Mie-Gru¨neisen equation of state parameters for the projectile, Al 5083-H116, and the perforated plate [17].

Material	C_0 (m/s)	S_1	S_2	S_3	γ_0

Steel 4340	4570	1.49	0	0	1.93
Al 5083-H116	0.0261	0.263	-0.349	0.147	1.68
Steel Armox 500T	4570	1.49	0	0	1.93

The *MAT_JOHNSON_COOK (015) material model is used in the finite element simulations to accurately represent the constitutive behavior of the perforated plate, aluminum plate, and projectile. This model incorporates failure criteria, strain rate effects (which increase strength), damage effects, and thermal effects [14]. In the Johnson-Cook material model, the dynamic Von Mises flow stress σ_0 is given by [16].

$$\sigma_0 = (A + B\,\varepsilon_P^n)\left(1 + C\,ln\frac{\dot{\varepsilon}_P}{\dot{\varepsilon}_0}\right)\left[1 - \left(\frac{T-T_r}{T_m-T_r}\right)^m\right] \quad (2)$$

Table **2**. The J-C damage model is given by [17]:

$$\varepsilon_f = [D_1 + D_2 exp(D_3\sigma^*)]\left(1 + D_4 \ln\frac{\dot{\varepsilon_P}}{\dot{\varepsilon_0}}\right)(1 + D_5 T^*) \quad (3)$$

where ε_f is the failure strain; D_1-D_5 are the material parameters; and $\sigma^* = {}^{\sigma_m}/_{\sigma_{eff}}$ is the ratio of the mean compression (σ_m) to the equivalent Von-Mises stress (σ_{eff}). Johnson-Cook damage model parameters are given in Table **3**.

Johnson-Holmquist (JH-2) ceramic model (Mat_110) [18] was implemented to study the brittle failure characteristics of silicon carbide (SiC) ceramic under high-velocity impact conditions. This model accounts for the material's pressure-dependent strength, damage evolution, and strain-rate effects. The key parameters governing the JH-2 model for SiC ceramic are provided in Erosion strain = 2 is dimensionless, as LS-DYNA defines it relative to effective plastic strain.

Table 4 [19]. The normalized equivalent stress in the JH-2 model is mathematically given by:

where A is the yield strength, B is the hardening modulus, ε_P is the equivalent plastic strain, n is the strain-hardening exponent, C is the strain-rate sensitivity coefficient, $\dot{\varepsilon}_P/\dot{\varepsilon}_0$ is the dimensionless plastic strain rate, T_m is the temperature melting and T_r is reference temperatures, m is the thermal softening coefficient.

This model effectively characterizes the material behavior under high strain rates, large deformations, and thermal effects, making it suitable for ballistic impact simulations. The parameters of the Johnson-Cook plasticity model, which define the material behavior under dynamic loading conditions, are provided in

$$\sigma^* = \sigma_i^* - D(\sigma_i^* - \sigma_f^*). \quad (4)$$

The stresses are rendered dimensionless by normalizing them to the equivalent stress at the Hugoniot Elastic Limit (HEL). This normalization can be mathematically expressed as:

$$\sigma^* = {}^{\sigma}/_{\sigma_{HEL}}. \quad (5)$$

The normalized equivalent strength of intact ceramic (σ_i^*) and fractured ceramic (σ_f^*) is given by Eqs. (6) and (7):

$$\sigma_i^* = A(P^* + T^*)^N\left[1 + CLn\left({}^{\dot{\varepsilon}}/_{\dot{\varepsilon_\circ}}\right)\right], \quad (6)$$

$$\sigma_f^* = B(P^*)^M\left[1 + CLn\left({}^{\dot{\varepsilon}}/_{\dot{\varepsilon_\circ}}\right)\right], \quad (7)$$

The damage is considered to progressively accumulate as a result of incremental plastic deformation (ε_P):

$$D = \sum \frac{\Delta\varepsilon_P}{\Delta\varepsilon_P^f} \quad (8)$$

$$\varepsilon_p^f = D_1(P^* + T^*)^{D_2}. \quad (9)$$

Table 2. Material parameters for the projectile and the armor plates [17].

Parameter	Symbol	Unit	Al 5083-H116	Projectile core Steel 4340	Steel Armox 500T
Density	ρ	(g/cm3)	2700	7850	7850
Shear modulus	G	GPa	26.4	80	75.6
Specific heat	Cp	J/kg K	910	477	455
Johnson–Cook plasticity model parameters					
Initial yield stress	A	MPa	167	1900	1372.5
Strain hardening coefficient	B	MPa	596	1100	835
Strain hardening exponent	n		0.551	0.3	0.2467
Thermal softening exponent	m		0.859	1	0.84

Melting temperature	T_m	K	893	1800	1800
Reference temperature	T_{re}	K	293	300	293
Strain rate coefficient	C		0.001	0.05	0.0617
Reference strain rate	$\dot{\varepsilon_0}$	1/s	1	0.001	1

Table 3. Johnson-Cook damage model parameters for projectile core and armor plates [17][20].

Material	D_1	D_2	D_3	D_4	D_5
Steel Armox 500T	0.04289	2.1521	-2.7575	-0.0066	0.86
Projectile core	0.05	3.44	-2.12	0.002	0.61
Steel 4340					
Al 5083-H116	0.0261	0.263	-0.349	0.147	1.68

where $\Delta\varepsilon_P$ is the incremental effective plastic strain, $\Delta\varepsilon_P^f$ is the failure strain, and D1 and D2 are material constants. Also, A, B, C, M, and N are material constants, while D represents the damage factor, constrained within the range ($0 \leq D \leq 1$). The pressure model is expressed as:

$$P = K_1\mu + K_2\mu^2 + K_3\mu^3 + \Delta P, \quad (10)$$

where μ is the compressibility factor and K1, K2, and K3 are constants. The instantaneous geometric strain criterion is chosen to delete the distorted elements of the ceramic. Erosion strain = 2 is dimensionless, as LS-DYNA defines it relative to effective plastic strain.

Table 4. JH-2 material and model constants for SiC [19].

Parameters	Value
Density, ρ (g/cm3)	3.18
Bulk modulus, K_1 (GPa)	217.2
Pressure constant, K_2 (GPa)	0.0
Pressure constant, K_3(GPa)	0.0
Bulking factor, β	1.0
Shear modulus, G (GPa)	183.8
Hugoniot elastic limit (HEL) (GPa)	14.7
Intact strength constant, A	0.96
Strain rate constant, C	0.0045
Fracture strength constant, B	0.35
Fracture strength exponent, M	1.0
Maximum fracture strength ratio	1.0
Hydro tensile limit, T (GPa)	0.42
Damage constant, D1	0.48
Damage constant, D2	0.48
Intact strength constant, N	0.65

The Kevlar fiber is simulated using the Composite Damage Model (*MAT_22) in LS-DYNA, incorporating orthotropic constitutive relations to define the stress-strain behavior. The failure mechanisms incorporated into this model, with an added erosion criterion, are classified into four primary categories: tensile failure of the matrix. Compressive failure of the matrix. Tensile failure of the fibers. Compressive failure of the fibers. The corresponding material parameters utilized in the *MAT_22 model are provided in Table 5. The projectile is modeled with a simplified geometry, featuring a diameter of 10.9 mm and a length of 31.8 mm. It is assigned an initial incident velocity of 820 m/s. The projectile head has a curvature radius of 28.62 mm, and the material is designated as Steel 4340, which is widely used in ballistic applications due to its high strength and toughness (Fig. 1.a). Considering the symmetry of the perforated plate and the projectile, only a half-model was established to reduce computational effort. The projectile was meshed with a solid Mesher with an element size of 0.6 mm (Fig. 1b).

The perforated plate was meshed in two zones: the projectile contact zone and the outer zone. The mesh size increases in the radial direction from the projectile contact zone to the outer zone, ranging from 0.7 to 1.9 mm (Fig. 2). The ceramic layer consists of 16 silicon carbide tiles as a front layer, where the geometric configuration of the ceramic tile is shown in Fig. 3. The zigzag ceramic and zigzag aluminum layers were meshed using a solid Mesher with element sizes of 0.6 mm and 1.8 mm. The composite backing layer of aluminum/Kevlar was meshed as illustrated in Fig. 4. A uniform element size of 0.7 mm was applied to the central region, which measures 13 mm × 13 mm, with the element size gradually increasing further from this central zone. Throughout the analysis, an FE size of 0.7 mm was maintained in the thickness direction. A mesh convergence study confirmed stable residual velocity and penetration depth predictions at element sizes of 0.6–0.7 mm in critical zones. The in-plane dimensions of both the front (ceramic) and backing layers were set to 200 mm × 200 mm. The four faces at the edges of the target plate were clamped by assigning zero displacements and rotations in three directions. FE mesh used hexahedral elements (0.6–0.7 mm in contact zones), ~368750 elements, and ~327945 nodes. Half-symmetry reduced computational effort.

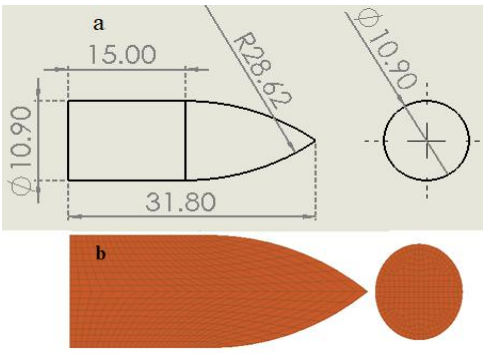

Fig. 1. (a) Projectile dimensions (mm), (b) Simulation model of the projectile.

Table 5. Ortho model parameters of Kevlar [18].

Parameters	ρ (kg/m³)	EA (GPa)	EB (GPa)	EC (GPa)	PRBA	PRCA	PRCB	GAB (GPa)
Kevlar	1440	35	35	8.33	0.0045	0.044	0.044	0.35
Parameters	GBC (GPa)	GCA (GPa)	Alph	Kfail (GPa)	Aopt	Macf	Sc (GPa)	Xt (GPa)
Kevlar	0.32	0.32	0	2.2	1.0	3	0.025	0.725
Parameters	Yt (GPa)	Yc (GPa)	Sn (GPa)	Syz (GPa)	Szx (GPa)	-	-	-
Kevlar	0.725	0.69	9.0	1.08	1.8	-	-	-

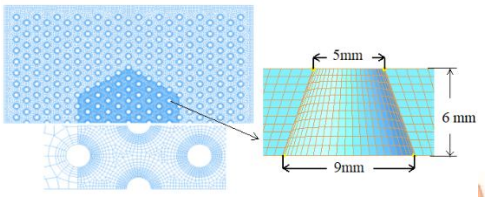

Fig. 2. Simulation model of the perforated plate.

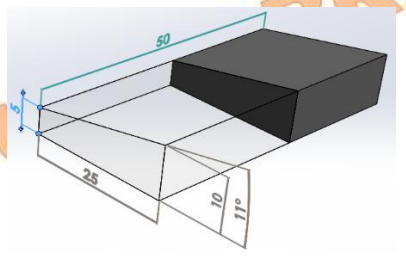

Fig. 3. Geometric configuration of the ceramic tile (mm).

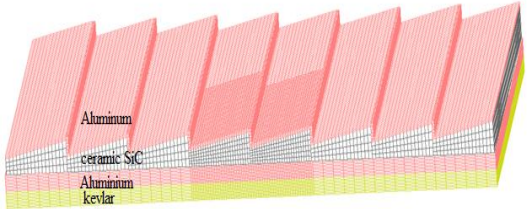

Fig. 4. Simulation model of the base armour (Zigzag Aluminium /ceramic/Aluminium/Kevlar).

Eroding surface-to-surface contact was utilized in the simulation to model interactions between the projectile, perforated plate, and the multilayer structure consisting of zigzag aluminum, zigzag ceramic, aluminum, and Kevlar. A zero-velocity boundary condition was applied to the four vertices of the perforated plate.

2.2. Verification of LS-Dyna Model

This section validates the accuracy of the current LS-DYNA model by comparing its simulation results with both experimental and computational data reported by Cao et al. [18]. A finite element (FE) model was created for the projectile and the lightweight multilayer composite armor. The components of the composite target, from the impact surface to the back surface, include 6061 aluminum alloy (1 mm), Al2O3 ceramic (14 mm), TC4 titanium alloy (4 mm), Kevlar (5 mm), and TC4 titanium alloy (3 mm). The obtained results are subsequently compared with the experimental findings reported by Cao et al. [18]. The accuracy of the current simulation is evaluated based on the details of the projectile impact, the residual velocity curve (Fig. 5), and the internal energy curve of the ceramic (Fig. 6).

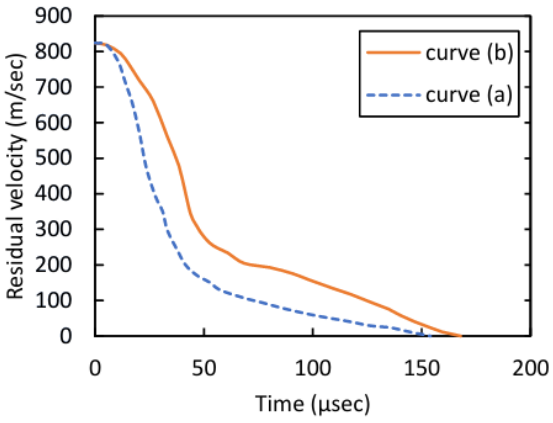

Fig. 5. The residual velocity curve (a) present finite element (FE) model, and (b) a finite element (FE) model [18].

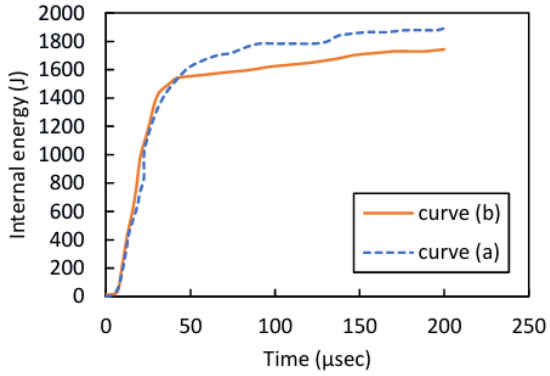

Fig. 6. The eroded internal energy of the ceramic layer curve (a) present finite element (FE) model, and (b) a finite element (FE) model [18].

The simulation results regarding residual velocity, penetration depth, and the ballistic performance of each component are consistent with the experimental and numerical findings, as shown in Fig. 7. Penetration depth: Experimental = 16.2 mm, Simulation = 15.5 mm. These metrics demonstrate excellent agreement beyond visual figure comparison. Residual velocity: 12.7mm AP projectile after multi-layer composite: experimental and simulated = 0 m/s (non-penetrating).

This simulation accurately depicts the penetration process of the 12.7 mm AP projectile through lightweight multilayer composite armor, aligning well with the actual test results reported by Cao et al. [18].

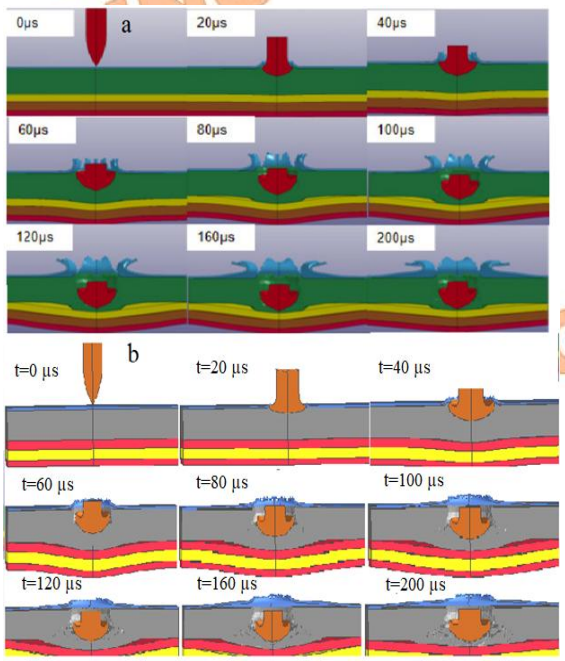

Fig. 7. Simulation of the penetration process over a time span of (0-200 μs). (a) study [18] and (b) the present study.

2.3. Results and Discussion

This section aims to validate the developed finite element model by comparing the numerical simulation results with available experimental ballistic data, ensuring the reliability and predictive accuracy of the LS-DYNA simulations. Initially, the impact of a 12.7 mm AP projectile on base armor (6061 aluminum alloy, Al2O3 ceramic, TC4 titanium alloy, Kevlar, and TC4 titanium alloy) was simulated using the commercial finite element code LS-Dyna to validate the model (Fig. 7). Subsequently, the impact of a 12.7 mm bullet on a 6 mm thick perforated plate, instead of the 8 mm thickness used in previous studies, was simulated to determine the geometry of the proposed perforated plate. As a result, the projectile velocity decreased from 820 to 600 m/s when the bullet struck the center of the hole (the critical case) after conical holes were replaced with cylindrical ones. A numerical study of the components of the protection system was conducted to characterize the ballistic performance of each component and its contribution to stopping the bullet.

2.4. Perforated Plate Geometry

The hole patterns were developed based on a theoretical analysis of a probabilistic model [21], which facilitated the identification of optimal perforation parameters. These perforated steel plates are designed to generate bending stresses that destabilize the projectile, thereby decreasing its penetrating capability. The probabilistic model aims to determine the optimal hole arrangement and spacing to achieve maximum weight reduction while preserving or improving protective performance. This approach is based on the principle that bending stress is induced when a projectile impacts both within a hole and in a designated area outside it, a phenomenon influenced by edge effects. Key perforation parameters include the hole diameter (R), the center-to-center spacing between holes (T), the width (δ) of the surface area that promotes projectile fragmentation or failure, and the surface area (S_f) where an impact can penetrate the perforated steel plate without causing projectile deflection or fragmentation (Fig. 8).

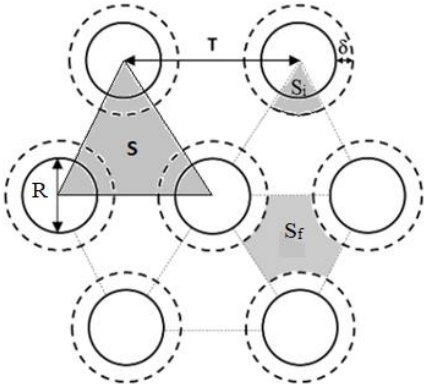

Fig. 8. Illustration of the Regular Triangular Perforation Pattern with a 60° Offset.

The first step in calculating the perforation layout was to determine the value of δ. This value was obtained using a formula derived from the conditions that give rise to the edge effect [21].

$$\delta / \frac{D}{2} \geq 0.35 \tag{11}$$

where D represents the diameter of the projectile core, and δ denotes the width of the overlap area, as defined in the probabilistic model.

$$\delta \geq 0.35\left(\frac{D}{2}\right) \tag{12}$$

$$\delta \geq 0.35\left(\frac{10.9}{2}\right) \Rightarrow \delta = 1.9mm$$

Next, the perforation hole diameter R was identified.

$$\delta = D - R \Rightarrow R = D - \delta = 10.9 - 1.9 = 9mm$$

The subsequent step in the analysis involved establishing the variation range for the perforation pattern T. The optimal value of T_{opt} was determined according to **Error! Reference source not found.**) ,**Error! Reference source not found.**) and **Error! Reference source not found.**), assuming that the probability of projectile penetration failure on the first shot was 0.95. The surface area conducive to projectile penetrator fragmentation (S_i) was calculated using Eq. (13):

$$S_i = 0.5 * \pi\left(\frac{R}{2} + \delta\right)^2 \tag{13}$$

$$S = \frac{T^2 * \sqrt{3}}{4} \tag{14}$$

where S represents the surface area between the centers of three holes.

The probability of projectile fragmentation (failure), denoted as P_n, for the first shot was calculated as follows:

$$P_n(1) = \left(\frac{S_i}{S_{opt}}\right) \tag{15}$$

$$P_n(1) = \left(\frac{S_i}{S_{opt}}\right) = \frac{2 * \pi\left(\frac{R}{2} + \delta\right)^2}{{T_{opt}}^2 * \sqrt{3}} \tag{16}$$

$$T_{opt} = \sqrt{\frac{2 * \pi\left(\frac{R}{2} + \delta\right)^2}{P_n(1) * \sqrt{3}}} \tag{17}$$

$$T_{opt} = \sqrt{\frac{2 * \pi(4.5 + 1.9)^2}{0.95 * \sqrt{3}}} = 12.4mm$$

The geometric configuration of the perforated plate is shown in Fig. 9. In this figure, the probability of an asymmetric impact that ensures projectile deflection is 0.95. Based on reference studies, the initial evaluation of the perforated plate's ballistic performance indicates that this design provides the highest likelihood of an asymmetric impact. The diameter of the holes in the current study matches the diameter of the cylindrical holes in previous studies, which confirmed ballistic effectiveness when the thickness of the perforated plate was 8 mm [20][22]. Additionally, the ballistic protection of the perforated plate is nearly non-existent when the impact point is at the center of the hole (the critical case). In this research, we aim to reduce the weight of the perforated plate by decreasing its thickness while ensuring ballistic protection under the critical scenario where the impact point is at the center of the perforation. Previous designs have excluded this condition when evaluating the ballistic performance of protection systems. This objective will be achieved by using a plate with a thickness of 6 mm instead of 8 mm and adopting conical perforations rather than cylindrical ones (Fig. 10).

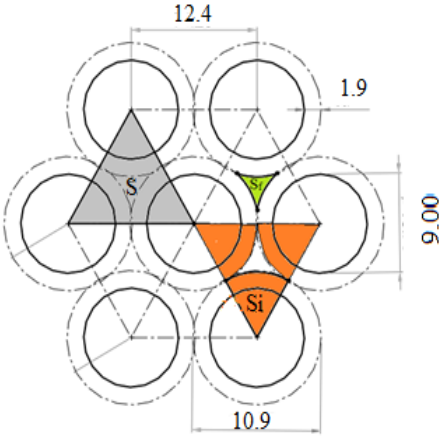

Fig. 9. The geometric configuration of the perforated plate mm.

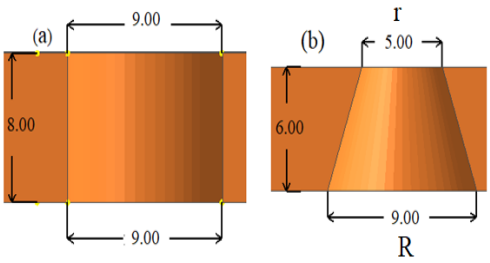

Fig. 10. (a) Geometry of cylindrical hole, (b) Geometry of conical frustum (proposed perforation) mm.

2.5. Numerical Study of Ballistic Response of Perforated Plates

There are two ballistic directions: the first is the large diameter of the hole (R), and the second is the small diameter of the hole (r) (Fig. 11). The performance of a perforated bullet is described based on the point of impact, which includes four scenarios: the bullet hits at the center of the perforation (critical case), the center of two holes, the center of three holes (symmetrical ballistic), and the side of the perforation (asymmetrical ballistic). Based on this, the ballistic processes of the four scenarios are modeled to determine the best ballistic direction for the perforated plate, as shown in Fig. 12.

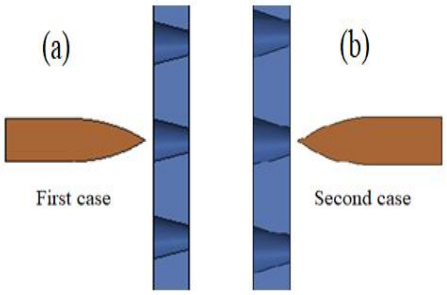

Fig. 11. Ballistic direction of perforated plate; (a) large diameter of the hole (R); (b) small diameter of the hole (r).

The results of the numerical study indicate that the optimal ballistic direction corresponds to the large diameter of the hole (first case) in Table 6.

Conical perforations induce asymmetric bending and higher projectile deformation, improving ballistic resistance and enabling weight reduction.

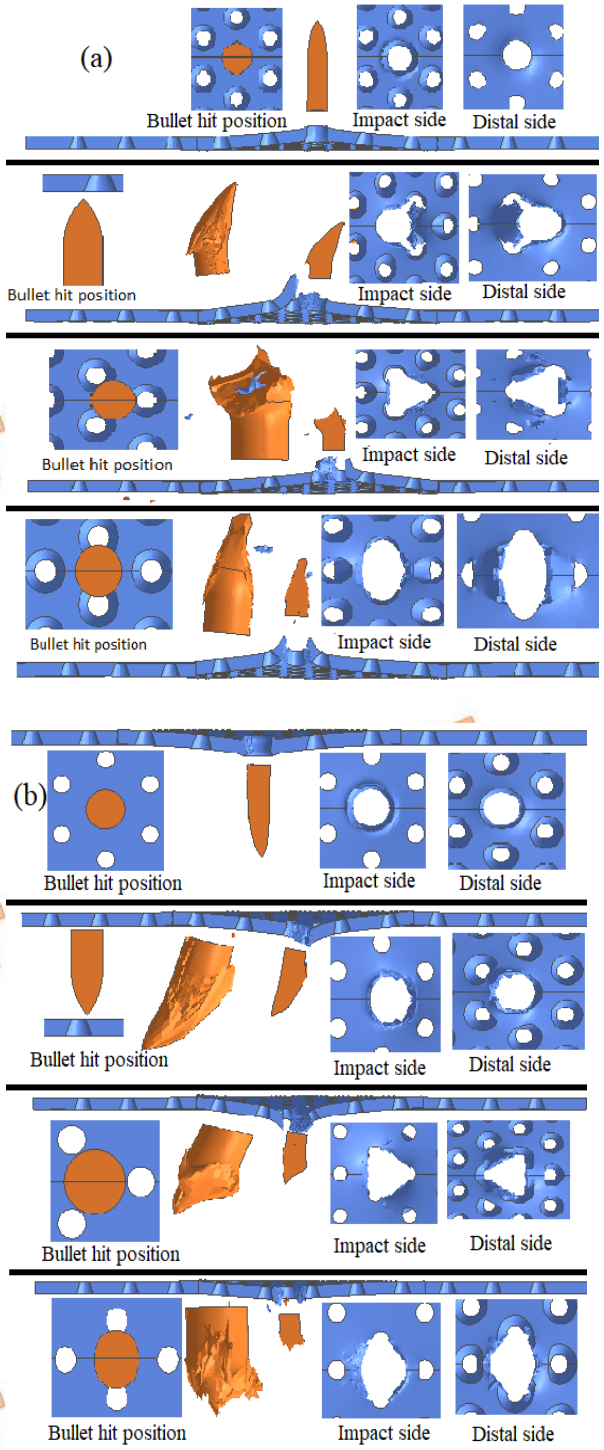

Fig. 12. Numerical study (four scenarios for the impact point) for perforated plate (a) First case (b) The second case.

Table 6. Ballistic performance of perforated plate depending on impact direction. First case: impact along large diameter (R); Second case: impact along small diameter (r).

Initial velocity (m/sec)	Bullet hit position	Residual velocity (m/sec)	
		First case	The second case
820	Center of hole	554	596
820	Side of hole	437	486
820	Center of three	415	442

	holes		
820	Middle of two holes	436	561

2.6. Optimization of Optimal Thickness for Aluminum Plate and Kevlar Layer

To achieve the optimal balance between ballistic performance and practical constraints, such as residual projectile velocity, weight, penetration depth, and cost, a series of experiments was designed and modeled. The experimental setup is illustrated in Table 7, where the two key factors, thickness of the aluminum plate (h_{Al}) and the Kevlar layer (h_K) were varied systematically Table 8, the projectile velocity was 600 m/s when the bullet struck the center of the hole (the critical case).

Table 7. Response surface methodology builds information.

File Version	13.0.5.0		
Study Type	Response Surface	Subtype	Randomized
Design Type	I-optimal	Point Exchange	Runs 16.00
Design Model	Quadratic		Blocks No Blocks

Table 8. Optimization factors information.

Factor	Name	Units	Type	Minimum	Maximum
A	Thickness (Al)	mm	Numeric	3.00	7.00
B	Thickness (k)	mm	Numeric	3.00	10.00

Using LS-Dyna software, simulations were conducted across multiple scenarios to assess the impact of different thickness configurations. The results, summarized in Table 10. The data were analyzed using the Response Surface Methodology (RSM), and an I-optimal design was implemented using Design-Expert v13.0.5.0 to determine the optimal solution. The numerical analysis revealed that the optimal thickness values were $h_{AL} \approx 5.5\,mm$ for the aluminum plate and $h_K \approx 5\,mm$ for the Kevlar layer (Fig. 13).

Table 9. Responses Information.

Response	Name	Units	Observations	Minimum	Maximum	Mean	Std. Dev.	Ratio
R1	weight	gr	16.00	1966	2879	2335.81	257.10	1.46
R2	R-velocity	m/sec	16.00	0	130	37.79	54.39	N/A
R3	displacement	mm	16.00	29.4	88.6	50.61	24.47	3.01
R4	cost	$	16.00	1364	3886	2493.00	827.79	2.85

Table 10. The design (Actual) by the design of experiments (RSM- I-optimal) for base armour

	Factor 1	**Factor 2**	**Response 1**	**Response 2**	**Response 3**	**Response 4**
Run	A: thickness (Al)	B: thickness (k)	weight	R-velocity	displacement	cost
	mm	mm	gr	m/sec	mm	$
1	3	10	2331	40.7	49.2	3613
2	7	5	2514	0	34.2	2183
3	6	4	2304	0	29.4	1773
4	5	7	2386	0	33.4	2727
5	4	4	2030	76	69	1637
6	5	10	2605	0	34.3	3749
7	5	3	2094	114	88.6	1364
8	3	5	1966	130	88	1910
9	3	5	1966	130	88	1910
10	5	7	2386	0	33.4	2727
11	6	8	2596	0	31.7	3136
12	5	3	2094	114	88.6	1364
14	7	10	2879	0	30.2	3886

15	4	8	2322	0	44.1	2999
16	7	5	2514	0	34.2	2183

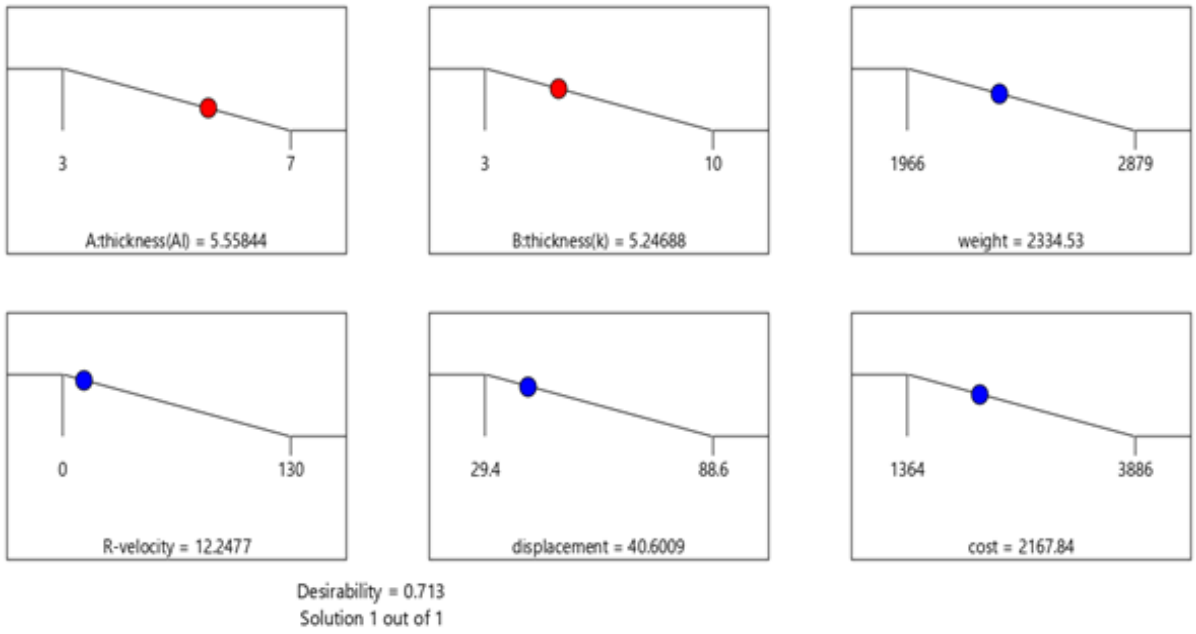

Fig. 13. Optimal numerical solution; optimal thickness (h_{Al}: Aluminum), (h_K: Kevlar).

The geometry and configuration of the corresponding protection system are depicted in (Fig. 14). These values demonstrate the best trade-off among the four evaluated criteria, ensuring effective ballistic protection while minimizing weight and cost.

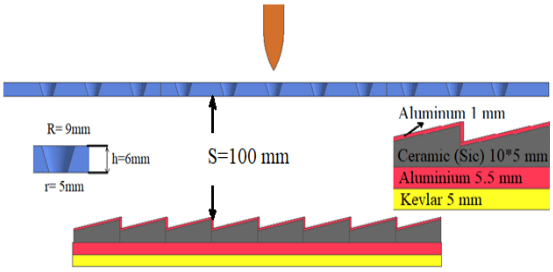

Fig. 14. Configuration and geometry of the protection system.

2.7. Numerical Study of Ballistic Response of Protection System

To describe the ballistic performance of the protection system, the numerical study included two scenarios. In the first scenario, where the impact point was on the side of the hole (asymmetric impact), the projectile deviated from its original trajectory after passing through the perforated plate. This deviation reduced its energy, making it easier for the base armor to stop it (Fig. 15). Additionally, the projectile's velocity decreased to 423 m/s after penetrating the perforated plate (Fig. 16). There was also noticeable deformation and wear on the projectile's tip. The perforated plate contributed to a 74.6% reduction in the projectile's total kinetic energy (Fig. 17).

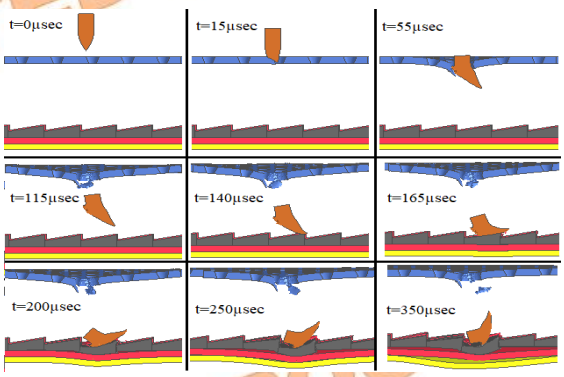

Fig. 15. Simulation of the penetration process (0-350 µs), bullet hit position: side of the hole.

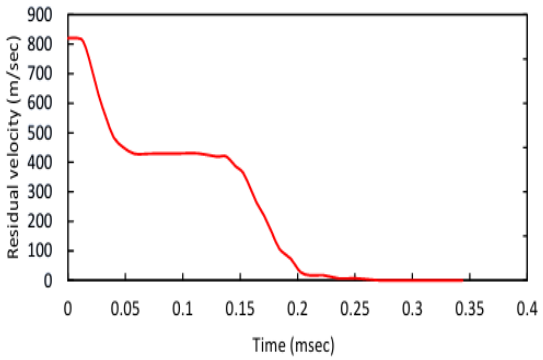

Fig. 16. Residual velocity curve of the projectile (bullet hit position: side of hole).

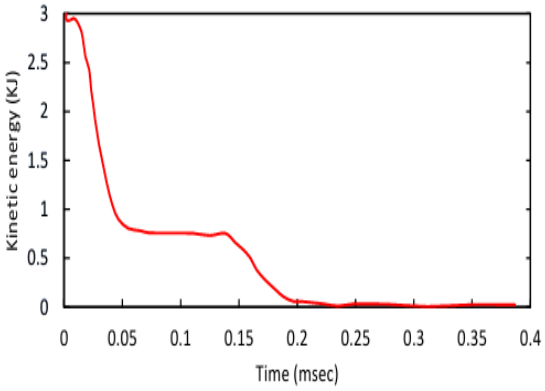

Fig. 17. Kinetic energy curve of the projectile (bullet hit position: side of the hole).

The sloping surface of the ceramic further contributed to the projectile's ricochet, thereby hindering its ability to penetrate.

In the second scenario (Fig. 18), where the impact point was aligned with the center of the conical hole (the critical case), the projectile's velocity decreased to 555 m/s after piercing the perforated plate (Fig. 19).

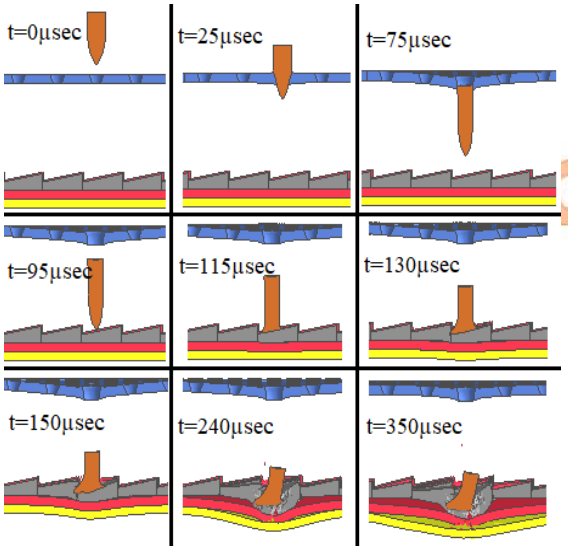

Fig. 18. Simulation of the penetration process (0-350 μs), bullet hit position: center of hole.

A noticeable deformation of the projectile was observed, with an elongation of 14.2 mm along its longitudinal axis. The perforated plate caused a 54% reduction in the projectile's total kinetic energy (Fig. 20). Additionally, the inclined ceramic surface further deflected the projectile from its trajectory, deforming its tip and mushrooming its structure, which effectively prevented the projectile from penetrating the protection system.

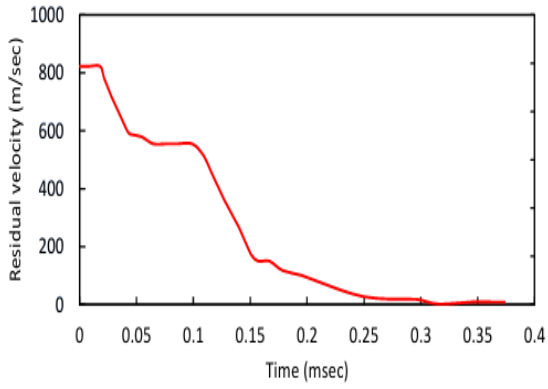

Fig. 19. Residual velocity curve of the projectile (bullet hit position: center of hole).

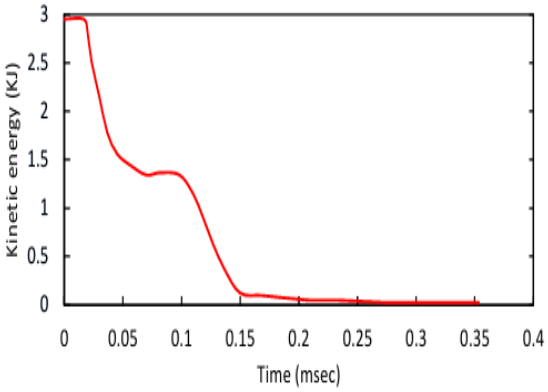

Fig. 20. Kinetic energy curve of the projectile (bullet hit position: center of hole).

The investigation revealed that the base armor alone was insufficient to prevent the penetration of a 12.7 mm (AP) projectile, resulting in a residual velocity of 194 m/s (Fig. 21).

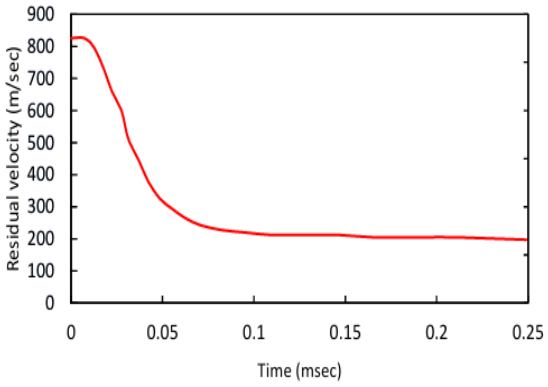

Fig. 21. Residual velocity curve of the projectile for base armor.

3. Conclusions

A numerical analysis was performed to evaluate the ballistic performance of a hybrid protection system, which consists of a perforated steel plate with conical holes and a base armor configuration made up of zigzag

aluminum, zigzag ceramic (SiC), aluminum, and Kevlar layers.

In this research, an asymmetric impact scenario was established to neutralize the projectile and weaken its penetration capability. This was achieved by placing a perforated armor plate in front of the primary armor layer. The perforated plate was designed with conical holes, resulting in a 25% reduction in thickness (from 8 mm, as referenced in previous studies, to 6 mm). This design change led to a significant reduction in the overall weight of the armor.

Additionally, an oblique impact scenario was simulated despite the vertical assembly of the armor system. This was achieved by employing ceramics with zigzag ballistic surfaces that induced a deflection in the projectile's trajectory. Consequently, the projectile failed to penetrate the protection system, demonstrating the effectiveness of this innovative design approach.

The optimized perforated plate design significantly enhanced ballistic performance, particularly when the projectile impacted the center of a hole. In this scenario, the projectile lost 54% of its kinetic energy after penetrating the plate. Unlike earlier designs that neglected this critical impact case during ballistic performance assessments, the new approach addresses this challenge, ensuring better energy dissipation and improved protection. The numerical study of four scenarios describing the ballistic performance of the perforated plate indicates that the maximum damage area is confined to the extent of three adjacent holes. All scenarios exhibited asymmetric ballistic interactions, except for the central impact case. These asymmetric impacts were a key factor in causing sufficient deflection and deformation of the projectile, allowing the base armor to effectively stop it. By improving the design of the perforated steel plate and utilizing ceramics with a zigzag surface structure, the projectile failure mechanism was altered, enabling the effective defeat of large-caliber projectiles.

The optimized perforated plate with conical holes has a total weight of 3240 g for a 300 × 300 mm target area (equivalent to approximately 3.6 kg/m^2). In comparison, the conventional perforated plate with cylindrical holes reported in [12] exhibits a surface density of about 5.29 kg/m^2, demonstrating a weight reduction of approximately 31.9% while maintaining and even enhancing ballistic performance in the critical case of impact at the perforation center.

Nomenclature

AP	Armor-Piercing
FEM	Finite Element Method
P	Represents the pressure
γ_0	Grüneisen coefficient
ρ_0	Initial density of the material
E	The absolute internal energy
μ	Specific volume
σ_0	Flow stress
G	Shear modulus
ε_P	Equivalent plastic strain
$\frac{\dot{\varepsilon}_P}{\dot{\varepsilon}_0}$	The dimensionless plastic strain rate
C_p	Specific heat
σ^*	The normalized equivalent stress
HEL	Hugoniot Elastic Limit
σ_i^*	The equivalent strength of an intact ceramic
σ_f^*	The equivalent strength of fractured ceramic
ε_p^f	Failure strain
K_1	Bulk modulus
K_2, K_3	Pressure constant
β	Bulking factor
N	Intact strength constant
RO	Mass density
EA	Young's modulus in a-direction.
EB	Young's modulus in b-direction.
EC	Ec, Young's modulus in c-direction.
PRBA	Poisson's ratio, ba.
PRCA	Poisson's ratio, ca.
PRCB	Poisson's ratio, cb.
GAB	Shear modulus, ab.
GBC	Shear modulus, bc.
GCA	Shear modulus, ca.
KFAIL	Bulk modulus of failed material

AOPT	Material axes option:
MACF	Material axes change flag for brick elements:
SC	Shear strength, ab plane
SN	Normal tensile strength
SYZ	Transverse shear strength
SZX	Transverse shear strength
XT	Longitudinal tensile strength, a-axis
YT	Transverse tensile strength, b-axis
YC	Transverse compressive strength, b-axis
P_n	The probability of projectile fragmentation
R	Diameter of the hole

Funding Statement

This research did not receive any specific grant from funding agencies in the public, commercial, or not-for-profit sectors.

Conflicts of Interest

The authors declare that they have no conflicts of interest.

References

[1] Hazell, P. J., 2022. *Armour: materials, theory, and design*. CRC Press.

[2] Biswas, K. and Datta, D., 2024. Oblique impact on ceramic–composite armor system: A numerical study, Proceedings of the Institution of Mechanical Engineers, Part L: Journal of Materials: Design and Applications, 238(7), pp. 1256–1267.

[3] Senthil, M. A. K., Madhu, V., Gupta, N. K., 2017. Oblique impact on single, layered and spaced mild steel targets by 7.62 AP projectiles. International Journal of Impact Engineering, 110, pp. 26–38.

[4] Taghipoor, H., Ghiaskar, A., Hosseinirad, H. and Hosseinirad M. A., 2025. Investigating the Behavior of Glass Fiber/Polyester Layered Composites Under Low-Velocity Impact. Journal of Composites Science, 9(9), p. 474.

[5] Sefidi, M., Taghipoor, H. and Damghani Nouri, M., 2024. Experimental crashworthiness analysis of corrugated-core sandwich panels under impact loading. Ships and Offshore Structures, 19(12), pp. 2190–2203.

[6] Taghipoor, H. and Peysayyar, R., 2023. Study on low-velocity impact response of kevlar/epoxy-polyurethane sandwich panels. Physica Scripta, 99(1), p. 15232.

[7] Peysayyar, R., Taghipoor, H. and Nouri, M. D., 2024. Sandwich panel behavior under low-velocity impact with polyurethane core. Proceedings of the Institution of Mechanical Engineers, Part L: Journal of Materials: Design and Applications, 238(7), pp. 1311–1330.

[8] Shokrieh, M. M. and Javadpour, G. H., 2008. Penetration analysis of a projectile in ceramic composite armor. Composite Structures, 82 (2), pp. 269–276.

[9] Jiang, A., Li, Y., Li, D. and Hou, H., 2022. Study on Anti-Penetration Performance of Semi-Cylindrical Ceramic Composite Armor against 12.7 mm API Projectile. *Crystals*, 12(10), p. 1343.

[10] Stanisławek, S., Morka, A. and Niezgoda, T., 2015. Pyramidal ceramic armor ability to defeat projectile threat by changing its trajectory. Bulletin of the Polish Academy of Sciences: Technical Sciences, 4.

[11] Balos, S., Howard, D., Brezulianu, A. and Labus Zlatanović, D., 2021. Perforated Plate for Ballistic Protection—A Review. Metals, 11(4), p. 526.

[12] Mubashar, A., Uddin, E., Anwar, S., Arif, N., Waheed Ul Haq, S. and Chowdhury, M. A. K., 2019. Ballistic response of 12.7 mm armour piercing projectile against perforated armour developed from structural steel. Proceedings of the Institution of Mechanical Engineers, Part L: Journal of Materials: Design and Applications, 233(10).

[13] Hao, W., Zhang, P., Xie, J., Hou, M., Wang, Z. and Bai, X., 2022. Investigation of impact performance of perforated plates and effects of the perforation arrangement and shape on failure mode. Engineering Failure Analysis, 140, p. 106638.

[14] Shi, A., Hang, X., Han, H. and *Xia*, K., 2024. Research on ballistic protection characteristics of perforated plates made of different steel materials for 12.7 mm penetrator projectile. *Journal of Physics: Conference Series*, 2808(1), p. 12007.

[15] Djordjevic, N., Vignjevic, R., Kiely, L., Case, S., Vuyst, T. D., Campbell, J. and Hughes, K., 2018. Modelling of shock waves in fcc and bcc metals using a combined continuum and dislocation kinetic approach. International Journal of Plasticity, 105, pp. 211–224.

[16] Fernando, P. L. N., Mohotti, D. and Remennikov, A., 2019. Behaviour of explosively welded impedance-graded

multi-metal composite plates under near-field blast loads. International Journal of Mechanical Sciences, 163, p. 105124.

[17] Xiao, Y. K., Wu, H., Fang, Q., Zhang, W. and Kong, X. Z., 2017. Hemispherical nosed steel projectile high-speed penetration into aluminum target. Materials & Design, 133, pp. 237–254.

[18] Cao, J., Lai, J., Zhou, J., Kang, N., Du, L. and Miao, Y., 2020. Experiments and simulations of the ballistic response of ceramic composite armors. Journal of Mechanical Science and Technology, 34, pp. 2783–2793.

[19] Hu, P., Cheng, Y., Zhang, P., Liu, J., Yang, H. and Chen, J., 2021. Ametal/UHMWPE/SiC multi-layered composite armor against ballistic impact of flat-nosed projectile. Ceramics International, 47(16), pp. 22497–22513.

[20] Radisavljevic, I., Balos, S., Nikacevic, M. and Sidjanin, L., 2013. Optimization of geometrical characteristics of perforated plates. Materials & Design, 49, pp. 81–89.

[21] Burian, W., Marcisz, J., Starczewski, L. and Wnuk, M., 2017. A probabilistic model of optimising perforated high-strength steel sheet assemblies for impact-resistant armour systems. Problemy Mechatroniki, Uzbrojenia, Lotnictwa i Inżynierii Bezpieczeństwa, 8.

[22] Balos, S., Grabulov, V., Sidjanin, L., Pantic, M. and Radisavljevic, I., 2010. Geometry, mechanical properties and mounting of perforated plates for ballistic application. Materials & Design, 31(6), pp. 2916–2924.